CHEMISTRY OF MATERIALS
Article
Cite This: Chem. Mater. 2017, 29, 9429-9435
pubs.acs.org/cm

Exploring Emerging Photovoltaic Materials Beyond Perovskite: The Case of Skutterudite

Yuan Yin,[†,‡,§] Yang Huang,[†,‡] Yelong Wu,[§] Guangde Chen,[§] Wan-Jian Yin,*[,†,‡] Su-Huai Wei,*[,∥] and Xingao Gong*[,⊥,#]

[†]Soochow Institute for Energy and Materials InnovationS (SIEMIS), College of Physics, Optoelectronics and Energy & Collaborative Innovation Center of Suzhou Nano Science and Technology, and [‡]Key Laboratory of Advanced Carbon Materials and Wearable Energy Technologies of Jiangsu Province, Soochow University, Suzhou 215006, China

[§]Department of Applied Physics and the MOE Key Laboratory for Nonequilibrium Synthesis and Modulation of Condensed Matter, Xi'an Jiaotong University, Xi'an, Shaanxi 710049, China

[∥]Beijing Computational Science Research Center, Beijing 100094, China

[⊥]Department of Physics, Key Laboratory of Computational Physical Science (Ministry of Education), State Key Laboratory of Surface Physics, Collaborative Innovation Center of Advanced Microstructures, Fudan University, Shanghai 200241, China

[#]Collaborative Innovation Center of Advanced Microstructures, Nanjing 210093, China

Supporting Information

ABSTRACT: Because of the stability and toxic issue of $CH_3NH_3PbI_3$, great efforts have been made to search emerging materials beyond perovskite. Most of the explorations are based on ns^2-containing compounds, because lone-pair s-orbital-derived antibonding states are believed to play a crucial role in unique properties of $CH_3NH_3PbI_3$. In this work, we chose skutterudite-structure $IrSb_3$ ($E_g \approx 1.3$ eV) as a case study to show that the strong antibonding character at valence band maximum (VBM) can appear without the contribution from lone-pair s orbital. First-principles calculations show that $IrSb_3$ possesses similar electronic properties as $CH_3NH_3PbI_3$: (i) ambipolar conductivity with much better electron and hole effective masses than that of $CH_3NH_3PbI_3$; (ii) strong optical absorption ($\sim 1 \times 10^4$ cm^{-1}); (iii) shallow dominating defects. More importantly, $IrSb_3$ is much more stable than $CH_3NH_3PbI_3$. Our work may shed light on searching new promising solar cell materials beyond ns^2-containing perovskite.

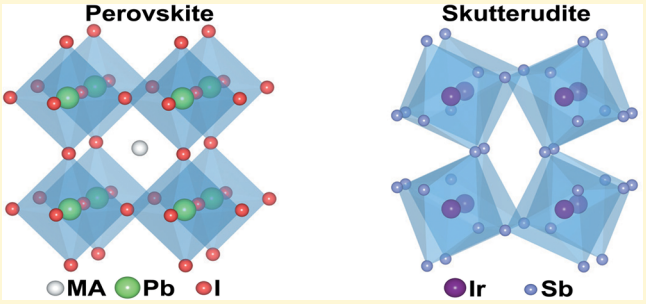

INTRODUCTION

Recent extensive research and rapid development of the organic−inorganic hybrid perovskite (OIHP) have made OIHP as the most promising materials for the next generation solar cells.[1−15] As a typical representative of OIHP, methylammonium lead iodide ($CH_3NH_3PbI_3$ or $MAPbI_3$) possesses superior optical and electronic properties, such as direct band gap with proper size, strong optical absorption, and long carrier lifetime and diffusion length.[16−20] Intensive efforts on chemical management and architecture optimization have been made in the past few years, and the certified power conversion efficiency of perovskite solar cells has jumped to 22.1%.[21]

As shown in Figure 1, distinguished from typical thin-film solar cell absorber GaAs, a valence band maximum (VBM) composed of strong antibonding states between Pb 6s orbital and I 5p in $MAPbI_3$ leads to high levels of band dispersion (small effective masses), ambipolar conductivity and defect tolerance, which are responsible for the long carrier lifetime and diffusion length thus high cell efficiency. Pb is among a few unique metal elements in periodic table whose outmost s electrons have low energy and are occupied when forming compounds. Such kinds of ions include Tl^{1+}, Sn^{2+}, Pb^{2+}, Sb^{3+},

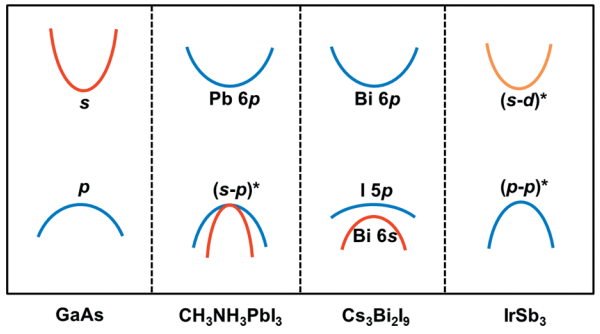

Figure 1. Illustrated band edge characters in representative materials for solar cell applications.

Received: August 19, 2017
Revised: October 13, 2017
Published: October 15, 2017

DOI: 10.1021/acs.chemmater.7b03507
Chem. Mater. 2017, 29, 9429−9435

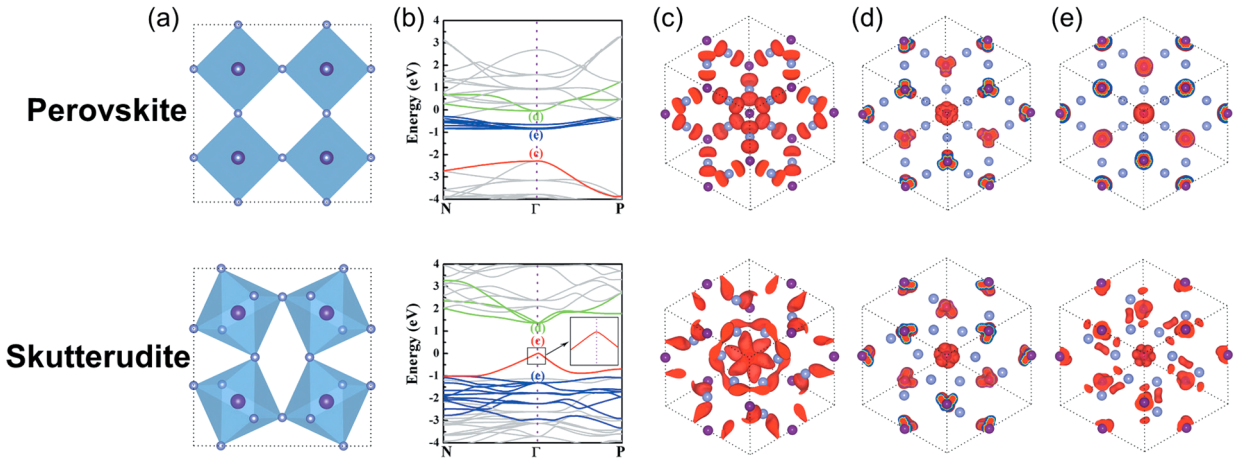

Figure 2. (a) Crystal structures, (b) band structures, and their respective partial charge densities of (c) VBM, (d) CBM, and (e) blue bands marked in the band structures in b. The almost linear band structure around VBM (5% length along Γ-N and Γ-P) of skutterudite is shown as inset in b.

and Bi^{3+}, where they only lose a p electron when they are ionized. The occupied s orbital, also called "lone-pair s electron/orbital", is the distinguished electronic configuration in OIHP. In conventional thin-film photovoltaic materials such as GaAs, VBM is mainly contributed from localized anion p orbital and thus hole effective mass is high. In O_h crystal symmetry of cubic perovskite, the low-lying lone-pair s electron has strong coupling with the state derived from splitting the anion p orbital at the R point, and thus the valence band close to VBM becomes dispersive, leading to the low hole effective mass and high VBM alignment responsible for defect tolerance.

Therefore, more and more efforts have recently been devoted to the exploration of alternative new perovskite, focusing on the ns^2-containing compounds.[22−25] The focus in the research is to identify new superior perovskite beyond $MAPbI_3$ that can overcome the stability and toxic issues associated with $MAPbI_3$. Recently, Slavney et al. successfully synthesized double perovskite $Cs_2AgBiBr_6$, which can be considered as the chemical mutation based on perovskite $CsPbI_3$, similar to the mutation from $CuInSe_2$ to $Cu_2ZnSnSe_4$. Unfortunately, the band gap of $Cs_2AgBiBr_6$ (~1.9 eV) is much larger than the optimal band-gap range for solar cell and the low-gap counterpart Cs_2AgBiI_6 is unstable.[26,27] Furthermore, the chemical mismatch of B-site atoms between Ag and Bi leads to indirect band gap and significantly changes the electronic characters near band edge.[28] Sun et al. suggested improved band gaps and optical absorption coefficients of $MABiSeI_2$ and $MABiSI_2$ by splitting the anions of $MAPbI_3$.[22] However, the anion-splitting compounds $MABiSeI_2$ and $MABiSI_2$ have been proven to be unstable and easily decomposed into secondary phases.[29]

As an alternative to perovskite structure, other works extend the search of lone-pair s compounds to nonperovskite phases.[24,30] So far, none of these new materials has approached the cell performance of $CH_3NH_3PbI_3$, partly because of the underlying key physics behind $CH_3NH_3PbI_3$, namely, the strong antibonding coupling character at the band edge does not exist. In cubic phase of $CH_3NH_3PbI_3$, I 5p orbitals split into singlet *a* and double-degenerate e states at R point of Brillouin zone. Singlet Pb 6s orbital has strong coupling with I 5p-derived a orbital due to the same symmetry. In other crystal structures with reduced symmetry, such kind of coupling was significantly reduced despite the existence of lone-pair *s* orbital. For example, in $CuSbS_2$ and $Cs_3Bi_2I_9$, the VBM is mainly I 5p character without strong Bi 6s contribution (Figure 1), which could also be seen from the flat upper valence band (large hole effective mass),[31] partly explaining their inferior cell performance. Those facts indicate that the antibonding character is more fundamental origin of superior photovoltaic properties than lone-pair s orbital.

In this paper, we show that the unique properties of halide perovskite, mainly the strong antibonding character at VBM, can be derived without contribution from lone-pair s orbitals. We have found that binary skutterudite $IrSb_3$ has similar electronic and optical properties of halide perovskite, such as proper band gap (~1.3 eV), small carrier effective masses (0.11 m_0 for electron and 0.07 m_0 for hole), strong optical absorption coefficient (~1×10^4 cm^{-1}), and shallow dominating defects. Most of those properties are derived from the antibonding character of its VBM, which has no lone-pair *s* contribution. Furthermore, covalent compound $IrSb_3$ is more stable than ionic halide perovskite. With less elemental compositions, the material growth and defect control in binary compounds are much easier than its ternary and multinary counterparts. Discovery of stable compound with strong antibonding character at VBM may open an alternative way for searching promising solar cell materials out of the scope of ns^2-containing elements.

METHODS

First-principles calculations were implemented to calculate electronic, optical and defect properties by using the Vienna Ab Initio Simulation Package (VASP) code[32,33] with the standard frozen-core projector augmented-wave (PAW) method.[34,35] For crystal structure calculation, we used generalized gradient approximation of Perdew, Burke, and Ernzerhof (PBE)[36] for the exchange-correction potential and for electronic structure of skutterudite, hybrid density functional (Heyd-Scuseria-Ernzerhof, HSE06) with exact exchange portion of 0.43 was used for band gap correction. The cutoff energy for basic wave functions was 280 eV. We have performed electronic structure calculations, such as band structure, density of states, and partial charge density based on the binary skutterudite $IrSb_3$ primitive cell containing 16 atoms with periodic boundary conditions. To simulate the formation of point defects, we have developed the supercell model and a defect is placed in this supercell. On the basis of a (256 atoms) supercell with the Γ point sampling, the defect calculations of $IrSb_3$ are performed by HSE06 with initial-PBE-then-HSE06 relaxed atomic structures. Spin−orbit coupling (SOC) was not included since our calculation show that SOC has negligible effect on electronic structure

DOI: 10.1021/acs.chemmater.7b03507
Chem. Mater. 2017, 29, 9429−9435

(Figure S2). Both the atomic positions and cell parameters are allowed to fully relax by minimizing the quantum mechanical force on each ion to be less than 0.02 eV/Å.

For the ionized defect α in the charge state q, its formation energy $\Delta H(\alpha, q)$ can be derived according to

$$\Delta H(\alpha, q) = E(\alpha, q) - E(\text{host}) + \sum_i n_i(E_i + \mu_i) + q(E_v + E_F) \quad (1)$$

Where $\Delta H(\alpha, q)$ is the total energy of the equivalent supercell with a defect α in the charge state q, E(host) is the total energy of the equivalent supercell in the absence of the defect, and the electron Fermi energy E_F is relative to the VBM of the host E_v.

RESULTS AND DISSCUSSION

Skutterudite compounds, discovered in 1845 at a town named Skutterude in Norway,[37] have chemical formula of binary phase MX_3 (M = Co, Rh, Ir, Ni, Fe and X = P, As, Sb). The crystal structure of binary skutterudite BX_3 is shown in the lower panel of Figure 2a. It can be considered as octahedral distortion from cubic perovskite structure $IrSb_3$, where A site is empty. During the distortion, four Sb atoms move to the center of the cube and the O_h symmetry of the cubic perovskite is reduced to tetragonal structure of the $Im\bar{3}$ symmetry resulting in a large void enclosed by MX_6 octahedron per four MX_3. Since 1990s, skutterudites have been studied as efficient thermoelectric materials. In thermoelectric applications, the focus have been on the compounds with low bandgaps (Table 1) such as CoP_3, $CoAs_3$, $CoSb_3$, $RhSb_3$, and $RhAs_3$, and the thermoelectric properties such as thermal and electrical conductivity.[37−40] The potential applications of skutterudite in photovoltaic field have never been investigated in particular to compounds like $IrSb_3$ which has larger band gap for better sunlight harvesting.

Table 1. Experimental Band Gaps of Binary Skutterudites in the Literatures[45−50]

	CoP_3	$CoAs_3$	$CoSb_3$	$RhAs_3$	$RhSb_3$	$IrSb_3$
E_g (eV)	0.43−0.45	0.69	0.04−0.63	0.8	0.8	1.18−1.4

Slack et al. measured the near-normal incidence reflectivity and estimated the band gap of 1.4 eV for $IrSb_3$.[41] Caillat et al. estimated band gap of 1.18 eV from electrical resistivity and Hall effect measurement.[42] Both of the values are within the optimal bandgap range for solar cell absorbers. In this study, the method of HSE06 hybrid functional[43,44] with exact exchange portion 0.43 is used to correct the band gap to 1.30 eV, close to experimental values as shown in Table 1. The HSE06 calculated lattice constant is 9.39 Å, in good agreement with experimental value of 9.25 Å.

Although the structural similarity between perovskite and skutterudite, the electronic structure relation between perovskite and skutterudite is unclear. The unit cell of cubic perovskite $IrSb_3$ contains four atoms and after distortion the unit cell becomes body-centered-cubic with 16 atoms. In reciprocal space, three M points and one Γ point in cubic BZ fold to the Γ point of body-centered-cubic Brillouin zone (Figure S3). In this study, we constructed perovskite $IrSb_3$ and intermediate structures between perovskite and skutterudite to investigate the electronic structure evolution from perovskite to skutterudite (Figure S4). As shown in Figure 2b, perovskite $IrSb_3$ has zero band gap and three parts of typical bands are highlighted, which are corresponding to the highlighted bands in skutterudite. In perovskite $IrSb_3$, red/blue/green bands are mainly from Sb/Ir/Ir atom. From perovskite to skutterudite, the Ir-centered Sb octahedra are tilted and the four nearby Sb vertex atoms are bonded as a square. During the tilt of the octahedra, the local number of coordination for Sb change from two to four while that for Ir does not change. Since blue and green bands are mainly contributed from Ir (Figure 2d, e), their energy levels do not change as significantly as the red bands, which originated from Sb 5p orbitals. When Sb−Sb is coming close, their antibonding pp bands move rapidly above Ir 5d bands and open a gap between antibonding Sb p bands and Ir-derived green bands in skutterudite (see Figure 2 and Figure S3 for details). Because of the strong antibonding character at the VBM, $IrSb_3$ has similar electronic structure as $CH_3NH_3PbI_3$, in particular a large valence band dispersion.

In $CH_3NH_3PbI_3$, large dispersion at VBM originates from strong coupling between Pb 6s state and I 5p-splitted a state, which underlines the crucial role of lone-pair s electron in this system. Here, charge analysis show that VBM of $IrSb_3$ is pp antibonding state without any contribution from Sb lone-pair 5s states (lower panel of Figure 2c). The calculated hole effective mass as shown in Table 2 is 0.07 m_0, much lower than the hole effective mass 0.31 m_0 for $CH_3NH_3PbI_3$. Enlarged band structure at inset in Figure 2c shows an almost linear energy band shape along both Γ-N and Γ-P direction. It is interesting that the p-p antibonding state can be much more dispersive than s-p antibonding state, indicating that the superior properties in ns^2-containing perovskite can appear in crystal structures other than perovskites and compounds without lone-pair s element. This will significantly expand the materials scope for emerging solar cell materials beyond perovskite.

Table 2. Calculated Effective Masses (m^*) of Electrons and Holes for Typical Solar Cell Absorbers $IrSb_3$, $CH_3NH_3PbI_3$, Si, GaAs, and CdTe

	$IrSb_3$	$CH_3NH_3PbI_3$	Si	GaAs	CdTe
m_e^*	0.11	0.35	0.26	0.07	0.09
m_h^*	0.07	0.31	0.29	0.34	0.28

Another interesting issue is that, thanks to the switch-on of s-e_g coupling in skutterudite structure,[49] the conduction band minimum (CBM) of $IrSb_3$ is mainly contributed from e_g obital of Ir 5d with strong coupling to Sb s orbital. Because of the contribution from delocalized s orbital, the lower conduction band is also dispersive and the calculated electron effective mass is 0.11 m_0. The effective mass in Table 2 show that (i) the electron and hole effective mass are balanced and thus $IrSb_3$ has bipolar conductivity similar to $CH_3NH_3PbI_3$; (ii) both electron and hole effective masses of $IrSb_3$ are much smaller than that of $CH_3NH_3PbI_3$.

Apart from ambipolar conductivity, high optical absorption is one of unique properties of hybrid perovskite, in which photogenerated carriers do not have to travel far in absorber layers to be collected at the contacts so that the nonradiative recombination rate is low. The calculated optical absorption of GaAs, $CH_3NH_3PbI_3$ and $IrSb_3$ are shown in Figure 3a. Previous theoretical studies show that $CH_3NH_3PbI_3$ has higher optical absorption than GaAs because $CH_3NH_3PbI_3$ has higher joint density of states and the optical absorption for $CH_3NH_3PbI_3$ is sp-p transition, whereas for GaAs, although it has p-s transition, its joint density of state is low. Our present calculations show that the strength of optical absorption in $IrSb_3$ is stronger than

DOI: 10.1021/acs.chemmater.7b03507
Chem. Mater. 2017, 29, 9429−9435

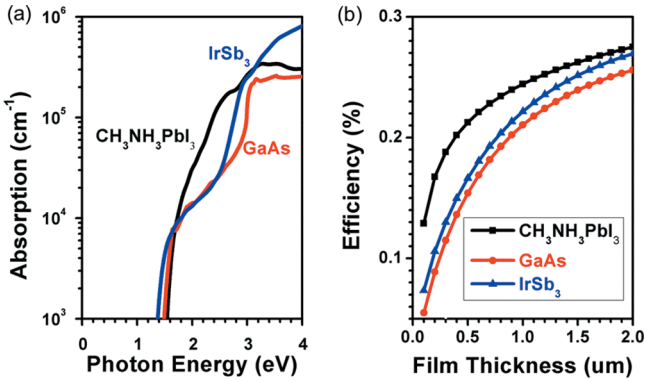

Figure 3. (a) Optical absorptions of $IrSb_3$, room-temperature phase $CH_3NH_3PbI_3$, and GaAs; and (b) the calculated maximum efficiencies (method developed by Yu et al.[51,52]) trend of $IrSb_3$, $CH_3NH_3PbI_3$, and GaAs as a function of film thickness.

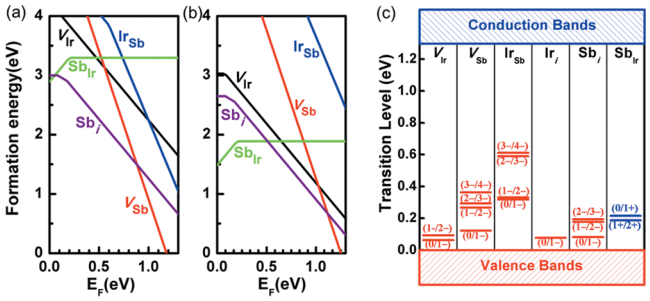

Figure 4. HSE06 calculated formation energies of native point defects in binary skutterudite $IrSb_3$ at chemical potentials (a) A (Ir-rich) and (b) B (Sb-rich), respectively. (c) Calculated transition levels of native defects in binary skutterudite $IrSb_3$.

that of GaAs but weaker than that of $CH_3NH_3PbI_3$. To investigate the impact of optical absorption on cell efficiency, the thickness-dependent maximum efficiency of $IrSb_3$ is calculated as shown in Figure 3b. At thin-layer end, the maximum efficiency of $IrSb_3$ is lower than that of $CH_3NH_3PbI_3$ but higher than that of GaAs, in consistent with their optical absorption strength. High optical absorption is often related to high density of states, whereas low carrier effective mass requires low density of states, so ideal solar cell absorber should have a good balance between optical absorption and carrier effective mass.

In $CH_3NH_3PbI_3$, due to strong level repulsion at the VBM, its energy is high, so the dominating acceptor defects are shallow, which is partially responsible for the long carrier lifetime and diffusion length. We have calculated the intrinsic point defects in binary skutterudite $IrSb_3$: vacancies (V_{Ir} and V_{Sb}), antisites (Ir_{Sb} and Sb_{Ir}) and interstitials (Ir_i and Sb_i). The number of defect types and competing secondary phases for binary $IrSb_3$ are less than that in multinary compounds, which may facilitate the material growth and defect controls in this kind of materials.

Thermodynamic equilibrium growth of $IrSb_3$ should satisfy

$$\mu_{Ir} + 3\mu_{Sb} = \Delta H(IrSb_3) = -2.56\ \text{eV} \quad (2)$$

$$\mu_{Ir} < 0 \quad (3)$$

$$\mu_{Sb} < 0 \quad (4)$$

where u_i is the chemical potential of constitute element referred to stable bulk phases of Ir and Sb and $\Delta H(IrSb_3)$ is the formation enthalpy of $IrSb_3$. To exclude secondary phases IrSb and $IrSb_2$, the following constraints must be satisfied:

$$\mu_{Ir} + \mu_{Sb} < \Delta H(IrSb) = -0.78\ \text{eV} \quad (5)$$

$$\mu_{Ir} + 2\mu_{Sb} < \Delta H(IrSb_2) = -2.21\ \text{eV} \quad (6)$$

The chemical potential of Ir (Sb) satisfying eqs 2−6 is calculated to be $-2.56\ \text{eV} < \mu_{Ir} < -1.50\ \text{eV}$, $-0.36\ \text{eV} < \mu_{Sb} < 0$.

In Figure 4, we show the calculated formation energies of these intrinsic point defects as a function of Fermi level at two chemical potentials limits A (Ir-rich, $\mu_{Ir} = -1.50$ eV, $\mu_{Sb} = -0.36$ eV) and B (Sb-rich, $\mu_{Ir} = -2.56$ eV, $\mu_{Sb} = 0$ eV), respectively. In comparison to $CH_3NH_3PbI_3$, the intrinsic defects of $IrSb_3$ have the following characters: (i) high formation energies. The formation energies of neutral defects, as shown in Figure 4a, are above 2 eV, which is much higher than the values in $CH_3NH_3PbI_3$ (~0 eV).[16] High defect formation energy in $IrSb_3$ means low defect density and high crystalline quality during materials growth, which could be beneficial for solar cell applications. (ii) intrinsic p-type. $IrSb_3$ is intrinsic p-type as shown in Figure 4a and b. The dominating acceptors (Sb_i, V_{Ir}) are shallow and dominating donor (Sb_{Ir}) is deep. To exclude the detrimental Sb_{Ir} and make better p-type, we suggested Ir-rich conditions during material growth in Figure 4a .

In Ir-rich conditions, dominating defects are Sb_i and V_{Ir}. As seen from Figure 4c, the (0/1−) transition levels for Sb_i and V_{Ir} are 82 and 62 meV, respectively. Those values are relatively shallow but a little larger than our calculated values for dominating defects in $CH_3NH_3PbI_3$ (<50 meV).[16] However, we should mention that previous calculations on $CH_3NH_3PbI_3$ are based on GGA while present calculations are based on HSE06 method. In general, HSE-calculated transition level is deeper than GGA-calculated ones. For example, the GGA-calculated transition levels of dominating defect Cu_{Zn} in CZTS is 120 meV while in hybrid functional methods, the calculated level is 200 meV.[53] In this sense, the transition levels of dominating defects in $IrSb_3$ should be comparable to those in $CH_3NH_3PbI_3$ and shallower than Cu_{Zn} in CZTS.

The major obstacle for commercialization of perovskite solar cell is the stability. For $CH_3NH_3PbI_3$, previous theoretical calculations demonstrate a very narrow region for equilibrium growth. Further calculations show that $CH_3NH_3PbI_3$ may be intrinsically unstable. In general, covalent compounds are more stable than ionic compounds. For ionic halide, the weak stability of $CH_3NH_3PbI_3$ is understandable especially in moisture environments. Here, we used bond energy, which is defined as the binding energy per bond, to quantitatively estimate the stability. The bond energies for Si, $IrSb_3$, GaAs, CdTe and $CH_3NH_3PbI_3$ are −2.72, −2.65, −2.01, −1.67, and −0.88 eV, respectively, as shown in Figure 5a. The trend from Si to GaAs to CdTe is typical trend from group IV semiconductor (more covalent) to III−V to II−VI semiconductors (more ionic). The bond energy of $IrSb_3$ is between Si and GaAs, indicating its strong covalency and stability. On the basis of bond energies, $CH_3NH_3PbI_3$ is more ionic than CdTe, explaining its weak stability.

To further verify the crystal stability of binary skutterudite $IrSb_3$, we choose six other common phases for AB_3 compounds (space group: *Fddd, pmnm, p312, C2/c, C2/m*, and $p3_112$) and compare their energies to the skutterudite structure. The results in Figure 5b show that skutterudite structure has much lower

DOI: 10.1021/acs.chemmater.7b03507
Chem. Mater. 2017, 29, 9429−9435

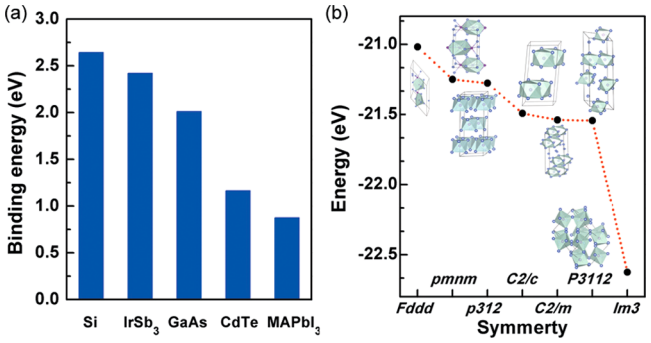

Figure 5. Calculated bond energies per bond of Si, $IrSb_3$, GaAs, CdTe, and $CH_3NH_3PbI_3$, and (b) the calculated energies of binary $IrSb_3$ in some common AB_3 compound structures.

energy than other competing structures, indicating the strong stability.

The ease of extrinsic doping in skutterudites may be another benefit for its utilization as solar cell absorber. The large void in crystal structures allow the filling of various extrinsic dopants including rare earth elements (La, Ce, Yb, Eu, Nd, and Sm),[54,55] alkaline earth metal elements (Ba, Sr, and Ca)[56,57] and others (Y, Sn, and Ge).[58,59] In thermoelectric research, high concentrations of both electron and hole have been reported for materials growth by extrinsic dopants,[60,61] indicating the tunability of carrier type and concentration in skutterudites properties. Further studies on extrinsic doping properties of $IrSb_3$ are underway.

CONCLUSIONS

In this work, we have proposed that the underlying feature of hybrid perovskite, namely, strong antibonding characters at VBM, which are responsible for unique properties such as small effective masses, ambipolar conductivity, and shallow dominating defect, can be inherited from materials beyond perovskite structure. Although $IrSb_3$, as a case studied in this work, does contain the Sb element with the lone-pair 5s electrons, the lone-pair s orbital has no contribution to antibonding states and thus may not be required. In this sense, this work underlines the strong antibonding character instead of lone-pair s orbital at VBM and may open a door for searching promising solar cell materials out of the scope of ns^2-containing compounds.

ASSOCIATED CONTENT

Supporting Information

The Supporting Information is available free of charge on the ACS Publications website at DOI: 10.1021/acs.chemmater.7b03507.

Band structure comparison of perovskite and skutterudite, with and without SOC, and evolution from perovskite to skutterudite (PDF)

AUTHOR INFORMATION

Corresponding Authors

*E-mail: wjyin@suda.edu.cn.
*E-mail: suhuaiwei@csrc.ac.cn.
*E-mail: xggong@fudan.edu.cn.

ORCID

Wan-Jian Yin: 0000-0003-0932-2789

Notes

The authors declare no competing financial interest.

ACKNOWLEDGMENTS

W.-J.Y. acknowledges stimulating discussion with Prof. Wenqing Zhang and Prof. Xun Shi, and funding support from National Key Research and Development Program of China under Grant 2016YFB0700700, National Natural Science Foundation of China (under Grants 51602211, 5172023, 11674237, and U1530401), Natural Science Foundation of Jiangsu Province of China (under Grant BK20160299). W.-J.Y. acknowledges the support from Suzhou Key Laboratory for Advanced Carbon Materials and Wearable Energy Technologies, China. The work was carried out at National Supercomputer Center in Tianjin, Lvliang, and Guangzhou, China, and the calculations were performed on TianHe-1(A) and TianHe-II.

REFERENCES

(1) Bretschneider, S. A.; Weickert, J.; Dorman, J. A.; Schmidt-Mende, L. Research update: physical and electrical characteristics of lead halide perovskites for solar cell applications. *APL Mater.* **2014**, *2*, 040701.
(2) Gao, P.; Grätzel, M.; Nazeeruddin, M. K. Organohalide lead perovskites for photovoltaic applications. *Energy Environ. Sci.* **2014**, *7*, 2448−2463.
(3) Snaith, H. J. Perovskites: the emergence of a new era for low-cost, high-efficiency solar cells. *J. Phys. Chem. Lett.* **2013**, *4*, 3623−3630.
(4) Kojima, A.; Teshima, K.; Shirai, Y.; Miyasaka, T. Organometal halide perovskites as visible-light sensitizers for photovoltaic cells. *J. Am. Chem. Soc.* **2009**, *131*, 6050−6051.
(5) Lee, M. M.; Teuscher, J.; Miyasaka, T.; Murakami, T. N.; Snaith, H. J. Efficient hybrid solar cells based on meso-superstructured organometal halide perovskites. *Science* **2012**, *338*, 643−647.
(6) Chung, I.; Lee, B.; He, J.; Chang, R. P.; Kanatzidis, M. G. All-solid-state dye-sensitized solar cells with high efficiency. *Nature* **2012**, *485*, 486.
(7) Liu, M.; Johnston, M. B.; Snaith, H. J. Efficient planar heterojunction perovskite solar cells by vapour deposition. *Nature* **2013**, *501*, 395.
(8) Park, N.-G. Organometal perovskite light absorbers toward a 20% efficiency low-cost solid-state mesoscopic solar cell. *J. Phys. Chem. Lett.* **2013**, *4*, 2423−2429.
(9) Burschka, J.; Pellet, N.; Moon, S.-J.; Humphry-Baker, R.; Gao, P.; Nazeeruddin, M. K.; Grätzel, M. Sequential deposition as a route to high-performance perovskite-sensitized solar cells. *Nature* **2013**, *499*, 316.
(10) McGehee, M. D. Perovskite solar cells: continuing to soar. *Nat. Mater.* **2014**, *13*, 845.
(11) Nie, W.; Tsai, H.; Asadpour, R.; Blancon, J.-C.; Neukirch, A. J.; Gupta, G.; Crochet, J. J.; Chhowalla, M.; Tretiak, S.; Alam, M. A.; et al. High-efficiency solution-processed perovskite solar cells with millimeter-scale grains. *Science* **2015**, *347*, 522−525.
(12) Li, X.; Bi, D.; Yi, C.; Décoppet, J.-D.; Luo, J.; Zakeeruddin, S. M.; Hagfeldt, A.; Grätzel, M. A vacuum flash−assisted solution process for high-efficiency large-area perovskite solar cells. *Science* **2016**, *353*, 58−62.
(13) Grancini, G.; D'Innocenzo, V.; Dohner, E.; Martino, N.; Srimath Kandada, A. R.; Mosconi, E.; De Angelis, F.; Karunadasa, H.; Hoke, E.; Petrozza, A. CH 3 NH 3 PbI 3 perovskite single crystals: surface photophysics and their interaction with the environment. *Chem. Sci.* **2015**, *6*, 7305−7310.
(14) Senthilarasu, S.; Fernández, E. F.; Almonacid, F.; Mallick, T. K. Effects of spectral coupling on perovskite solar cells under diverse climatic conditions. *Sol. Energy Mater. Sol. Cells* **2015**, *133*, 92−98.
(15) Stranks, S. D.; Nayak, P. K.; Zhang, W.; Stergiopoulos, T.; Snaith, H. J. Formation of Thin Films of Organic−Inorganic Perovskites for High-Efficiency Solar Cells. *Angew. Chem., Int. Ed.* **2015**, *54*, 3240−3248.

DOI: 10.1021/acs.chemmater.7b03507
Chem. Mater. 2017, 29, 9429−9435

(16) Yin, W.-J.; Shi, T.; Yan, Y. Unusual defect physics in CH3NH3PbI3 perovskite solar cell absorber. *Appl. Phys. Lett.* **2014**, *104*, 063903.
(17) Yin, W. J.; Shi, T.; Yan, Y. Unique properties of halide perovskites as possible origins of the superior solar cell performance. *Adv. Mater.* **2014**, *26*, 4653−4658.
(18) Frost, J. M.; Butler, K. T.; Brivio, F.; Hendon, C. H.; Van Schilfgaarde, M.; Walsh, A. Atomistic origins of high-performance in hybrid halide perovskite solar cells. *Nano Lett.* **2014**, *14*, 2584−2590.
(19) Yang, D.; Ming, W.; Shi, H.; Zhang, L.; Du, M.-H. Fast diffusion of native defects and impurities in perovskite solar cell material CH3NH3PbI3. *Chem. Mater.* **2016**, *28*, 4349−4357.
(20) Mosconi, E.; Amat, A.; Nazeeruddin, M. K.; Grätzel, M.; De Angelis, F. First-principles modeling of mixed halide organometal perovskites for photovoltaic applications. *J. Phys. Chem. C* **2013**, *117*, 13902−13913.
(21) http://www.nrel.gov/ncpv/images/efficiency_chart.jpg.
(22) Sun, Y.-Y.; Shi, J.; Lian, J.; Gao, W.; Agiorgousis, M. L.; Zhang, P.; Zhang, S. Discovering lead-free perovskite solar materials with a split-anion approach. *Nanoscale* **2016**, *8*, 6284−6289.
(23) Zhao, X.-G.; Yang, J.-H.; Fu, Y.; Yang, D.; Xu, Q.; Yu, L.; Wei, S.-H.; Zhang, L. Design of Lead-Free Inorganic Halide Perovskites for Solar Cells via Cation-Transmutation. *J. Am. Chem. Soc.* **2017**, *139*, 2630−2638.
(24) Saparov, B.; Hong, F.; Sun, J.-P.; Duan, H.-S.; Meng, W.; Cameron, S.; Hill, I. G.; Yan, Y.; Mitzi, D. B. Thin-film preparation and characterization of Cs3Sb2I9: A lead-free layered perovskite semiconductor. *Chem. Mater.* **2015**, *27*, 5622−5632.
(25) McClure, E. T.; Ball, M. R.; Windl, W.; Woodward, P. M. Cs2AgBiX6 (X= Br, Cl): new visible light absorbing, lead-free halide perovskite semiconductors. *Chem. Mater.* **2016**, *28*, 1348−1354.
(26) Slavney, A. H.; Hu, T.; Lindenberg, A. M.; Karunadasa, H. I. A bismuth-halide double perovskite with long carrier recombination lifetime for photovoltaic applications. *J. Am. Chem. Soc.* **2016**, *138*, 2138−2141.
(27) Hong, F.; Saparov, B.; Meng, W.; Xiao, Z.; Mitzi, D. B.; Yan, Y. Viability of Lead-Free Perovskites with Mixed Chalcogen and Halogen Anions for Photovoltaic Applications. *J. Phys. Chem. C* **2016**, *120*, 6435−6441.
(28) Savory, C. N.; Walsh, A.; Scanlon, D. O. Can Pb-Free Halide Double Perovskites Support High-Efficiency Solar Cells? *ACS Energy Lett.* **2016**, *1*, 949−955.
(29) Ge, J.; Grice, C. R.; Yan, Y. Cu-based quaternary chalcogenide Cu 2 BaSnS 4 thin films acting as hole transport layers in inverted perovskite CH 3 NH 3 PbI 3 solar cells. *J. Mater. Chem. A* **2017**, *5*, 2920−2928.
(30) Dufton, J. T.; Walsh, A.; Panchmatia, P. M.; Peter, L. M.; Colombara, D.; Islam, M. S. Structural and electronic properties of CuSbS 2 and CuBiS 2: potential absorber materials for thin-film solar cells. *Phys. Chem. Chem. Phys.* **2012**, *14*, 7229−7233.
(31) Park, B. W.; Philippe, B.; Zhang, X.; Rensmo, H.; Boschloo, G.; Johansson, E. M. Bismuth based hybrid perovskites A3Bi2I9 (A: methylammonium or cesium) for solar cell application. *Adv. Mater.* **2015**, *27*, 6806−6813.
(32) Kresse, G.; Hafner, J. Ab initio molecular dynamics for open-shell transition metals. *Phys. Rev. B: Condens. Matter Mater. Phys.* **1993**, *48*, 13115.
(33) Kresse, G.; Furthmüller, J. Efficient iterative schemes for ab initio total-energy calculations using a plane-wave basis set. *Phys. Rev. B: Condens. Matter Mater. Phys.* **1996**, *54*, 11169.
(34) Kresse, G.; Joubert, D. From ultrasoft pseudopotentials to the projector augmented-wave method. *Phys. Rev. B: Condens. Matter Mater. Phys.* **1999**, *59*, 1758.
(35) Blöchl, P. E. Projector augmented-wave method. *Phys. Rev. B: Condens. Matter Mater. Phys.* **1994**, *50*, 17953.
(36) Perdew, J. P.; Burke, K.; Ernzerhof, M. Generalized gradient approximation made simple. *Phys. Rev. Lett.* **1996**, *77* (18), 3865.
(37) Sales, B.; Mandrus, D.; Williams, R. K. Filled skutterudite antimonides: a new class of thermoelectric materials. *Science* **1996**, *272*, 1325.
(38) Lutz, H.; Kliche, G. Far-Infrared Reflection Spectra, Optical and Dielectric Constants, Effective Charges, and Lattice Dynamics of the Skutterudites CoP3, CoAs3, and CoSb3. *Phys. Status Solidi B* **1982**, *112*, 549−557.
(39) Kliche, G.; Lutz, H. Temperature dependence of the FIR reflection spectra of the skutterudites CoAs3 and CoSb3. *Infrared Phys.* **1984**, *24*, 171−177.
(40) Singh, D. J.; Pickett, W. E. Skutterudite antimonides: Quasilinear bands and unusual transport. *Phys. Rev. B: Condens. Matter Mater. Phys.* **1994**, *50*, 11235.
(41) Slack, G. A.; Tsoukala, V. G. Some properties of semiconducting IrSb3. *J. Appl. Phys.* **1994**, *76*, 1665−1671.
(42) Caillat, T.; Borshchevsky, A.; Fleurial, J. P. Preparation and thermoelectric properties of p-and n-type IrSb3. *AIP Conf. Proc.* **1994**, *316*, 31−34.
(43) Heyd, J.; Scuseria, G. E.; Ernzerhof, M. Hybrid functionals based on a screened Coulomb potential. *J. Chem. Phys.* **2003**, *118*, 8207−8215.
(44) Heyd, J.; Scuseria, G. E.; Ernzerhof, M. Erratum: "Hybrid functionals based on a screened Coulomb potential. *J. Chem. Phys.* **2006**, *124*, 219906.
(45) Ackermann, J.; Wold, A. The preparation and characterization of the cobalt skutterudites CoP3, CoAs3 and CoSb3. *J. Phys. Chem. Solids* **1977**, *38*, 1013−1016.
(46) Fleurial, J.-P.; Caillat, T.; Borshchevsky, A. In Skutterudites: an Update. In *Proceedings of the XVI International Conference on Thermoelectrics*; Dresden, Germany, Aug 26−29, 1997 ; IEEE: Piscataway, NJ, 1997; pp 1−11.
(47) Arushanov, E.; Respaud, M.; Rakoto, H.; Broto, J.; Caillat, T. Shubnikov−de Haas oscillations in CoSb 3 single crystals. *Phys. Rev. B: Condens. Matter Mater. Phys.* **2000**, *61*, 4672.
(48) Ishii, H.; Okazaki, K.; Fujimori, A.; Nagamoto, Y.; Koyanagi, T.; Sofo, J. O. Photoemission study of the skutterudite compounds CoSb3 and RhSb3. *J. Phys. Soc. Jpn.* **2002**, *71*, 2271−2275.
(49) Nagao, J.; Ferhat, M.; Anno, H.; Matsubara, K.; Hatta, E.; Mukasa, K. Electron tunneling experiments on skutterudite Co 1− x Fe x Sb 3 semiconductors. *Appl. Phys. Lett.* **2000**, *76*, 3436−3438.
(50) Nolas, G.; Slack, G.; Caillat, T.; Meisner, G. Raman scattering study of antimony-based skutterudites. *J. Appl. Phys.* **1996**, *79*, 2622−2626.
(51) Yu, L.; Zunger, A. Identification of Potential Photovoltaic Absorbers Based on First-Principles Spectroscopic Screening of Materials. *Phys. Rev. Lett.* **2012**, *108*, 068701.
(52) Yu, L.; Kokenyesi, R. S.; Keszler, D. A.; Zunger, A. Inverse Design of High Absorption Thin-Film Photovoltaic Materials. *Adv. Energy Mater.* **2013**, *3*, 43−48.
(53) Chen, S.; Walsh, A.; Gong, X. G.; Wei, S. H. Classification of lattice defects in the kesterite Cu2ZnSnS4 and Cu2ZnSnSe4 earth-abundant solar cell absorbers. *Adv. Mater.* **2013**, *25*, 1522−1539.
(54) Zhou, J.; Jie, Q.; Wu, L.; Dimitrov, I.; Li, Q.; Shi, X. Nanostructures and defects in nonequilibrium-synthesized filled skutterudite CeFe4Sb12. *J. Mater. Res.* **2011**, *26*, 1842−1847.
(55) Qiu, P.; Shi, X.; Qiu, Y.; Huang, X.; Wan, S.; Zhang, W.; Chen, L.; Yang, J. Enhancement of thermoelectric performance in slightly charge-compensated Ce y Co4Sb12 skutterudites. *Appl. Phys. Lett.* **2013**, *103*, 062103.
(56) Singh, D. J.; Du, M.-H. Properties of alkaline-earth-filled skutterudite antimonides: A (Fe, Ni) 4 Sb 12 (A= Ca, Sr, and Ba). *Phys. Rev. B: Condens. Matter Mater. Phys.* **2010**, *82*, 075115.
(57) Schnelle, W.; Leithe-Jasper, A.; Rosner, H.; Cardoso-Gil, R.; Gumeniuk, R.; Trots, D.; Mydosh, J.; Grin, Y. Magnetic, thermal, and electronic properties of iron-antimony filled skutterudites M Fe 4 Sb 12 (M= Na, K, Ca, Sr, Ba, La, Yb). *Phys. Rev. B: Condens. Matter Mater. Phys.* **2008**, *77*, 094421.
(58) Toda, M.; Sugawara, H.; Magishi, K.-i.; Saito, T.; Koyama, K.; Aoki, Y.; Sato, H. Electrical, Magnetic and NMR Studies of Ge-Based

DOI: 10.1021/acs.chemmater.7b03507
Chem. Mater. 2017, 29, 9429−9435

Filled Skutterudites R Pt4Ge12 (R= La, Ce, Pr, Nd). *J. Phys. Soc. Jpn.* **2008**, *77*, 124702.
(59) Nolas, G.; Kendziora, C.; Takizawa, H. Polarized Raman-scattering study of Ge and Sn-filled CoSb 3. *J. Appl. Phys.* **2003**, *94*, 7440−7444.
(60) Xi, L.; Qiu, Y.; Shi, X.; Zhang, W.; Chen, L.; Singh, D. J.; Yang, J. Defect-enhanced void filling and novel filled phases of open-structure skutterudites. *Chem. Commun.* **2015**, *51*, 10823−10826.
(61) Wang, S.; Sun, Y.; Yang, J.; Duan, B.; Wu, L.; Zhang, W.; Yang, J. High thermoelectric performance in Te-free (Bi, Sb) 2 Se 3 via structural transition induced band convergence and chemical bond softening. *Energy Environ. Sci.* **2016**, *9*, 3436−3447.

DOI: 10.1021/acs.chemmater.7b03507
Chem. Mater. 2017, 29, 9429−9435